ACS APPLIED MATERIALS & INTERFACES

Research Article

www.acsami.org

Lithium Titanate Epitaxial Coating on Spinel Lithium Manganese Oxide Surface for Improving the Performance of Lithium Storage Capability

Jili Li, Youqi Zhu, Lin Wang, and Chuanbao Cao*

Research Centre of Materials Science, Beijing Institute of Technology, Beijing 100081, China

Supporting Information

ABSTRACT: Spinel lithium titanate ($Li_4Ti_5O_{12}$, LTO) is applied as an epitaxial coating layer on $LiMn_2O_4$ hollow microspheres (LMO) through solvothermal-assisted processing. The epitaxial interface between LTO and LMO can be clearly observed by high resolution transmission electron microscopy (HR-TEM) and high angle annular dark field scanning transmission electron microscopy (HAADF-STEM) with atomic resolution images. The epitaxial coating cathode (EC-LMO@LTO) exhibits an excellent cyclability, thermal and rate capability for LIBs cathode due to the complete, thin LTO coating layer with strong adhesion to the host material. In addition, the small structure mismatch and high Li^+-ion mobility of LTO can be beneficial to forming an efficient tunnel for Li^+-ion transfer at the interface. It is suggested that EC-LMO@LTO can be recognized as a promising cathode material in electric vehicles (EVs) and plug-in hybrid electric vehicles (HEVs).

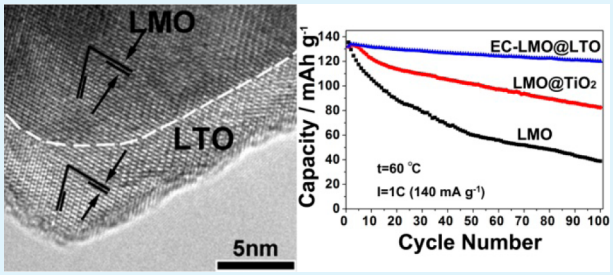

KEYWORDS: *heteroepitaxial structure, lithium titanate coating, Li-ion batteries, spinel lithium manganese oxide, solvothermal*

INTRODUCTION

Spinel $LiMn_2O_4$ is one of the most promising cathodes for large-scale Li-ion battery (LIB) applications in electric vehicles (EVs) and plug-in hybrid electric vehicles (HEVs) because of its high power density, low cost, abundant resources, environmental friendliness and good safety.[1−3] However, the main disadvantage that restricts the use of $LiMn_2O_4$ cathode is its fast capacity degradation during cycling, especially at elevated temperatures (>50 °C).[4,5] Substantial research has indicated that the fast capacity fading can be attributed to Mn dissolution into the electrolyte, the decomposition of the electrolyte on the electrode surface and Jahn−Teller (J−T) distortion effect of Mn^{3+} ions. Surface coating is recognized as an effective approach to minimize Mn dissolution and shield direct contact between $LiMn_2O_4$ cathode and the electrolyte for enhancing the performance.[6−18] Most of studies focused on modifying $LiMn_2O_4$ surface with inert metal oxides (Al_2O_3,[7−9] ZrO_2,[7,10] TiO_2,[11−13] ZnO,[14,15] etc.), fluorides[16−18] and phosphate.[19,20] However, the weak bonding between the coating layers and the host materials makes it possible for part of the coating layer to peel off from the electrode surface during the charge/discharge process, resulting in deterioration of electrochemical performance.[21] On the other hand, the apparent phase interface and large structural mismatch between the host and coating materials lead to numerous stacking faults and voids that can block forming a favorable tunnel for Li^+-ion diffusion.[22] Furthermore, these coating materials are insulators for Li^+-ion conduction, which limits improving the rate capability. Therefore, a new surface coating strategy and mechanism needs to be investigated to complement the above shortcomings.

Epitaxial coating, as a distinctive coating strategy, is mainly applied in the semiconductor field,[23,24] which is direct growth of a thin film on the surface of the host material with the same lattice orientation. It can lead to a dense and tight film to effectively suppress undesirable side reactions and the formation of voids between the host materials and the coating layer during cycling. Besides, there is the same lattice orientation and small lattice mismatch between the coating layer and the host material eliminating the apparent interface of coating layer and host material and decreasing the stacking faults to form an efficient tunnel for Li^+-ion diffusion.[22] Consequently, epitaxial coating may be an ideal strategy for improving the electrochemical performance of cathodes. Lithium titanate ($Li_4Ti_5O_{12}$, LTO), an important anode for LIBs, is a zero strain material (no structural change during Li insertion/extraction).[25−28] Moreover, LTO shares the same spinel structure with $LiMn_2O_4$. It is known the lattice parameters for $LiMn_2O_4$ and LTO are a = 8.357 and 8.248 Å, respectively. The lattice mismatch between $LiMn_2O_4$ and LTO is only 1.33%, which makes LTO possibly form an epitaxial coating layer on $LiMn_2O_4$. More importantly, LTO has a much higher Li^+-ion mobility, making the diffusion of Li^+ ions to the active material more easily for improving the rate

Received: July 3, 2014
Accepted: October 16, 2014
Published: October 16, 2014

Scheme 1. Preparation and Coating Process of LMO, LMO@TiO_2 and EC-LMO@LTO

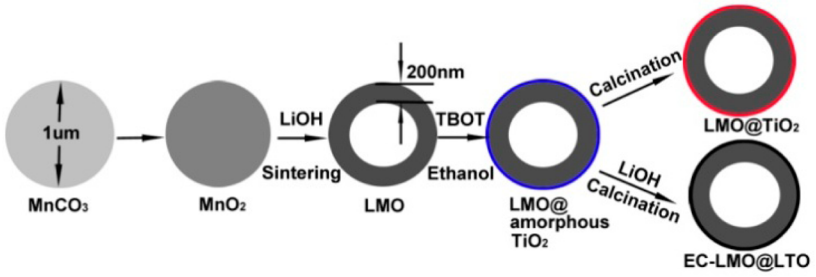

capability of the active material.[5] In this regard, it can be expected that a thin, complete and epitaxial LTO coating layer can enable significantly improving the cyclability, thermal stability and rate capability of $LiMn_2O_4$ cathodes.

In previous reports, a LTO coating layer established through traditional sol−gel technique on the host bulk cathodes cannot yield a thin, complete, uniform and robust coating layer, leading to electrochemical performance dissatisfactory.[29−34] Besides, they are mainly related to LTO nanoparticles randomly covering the surfaces of active materials. Moreover, very little work has been done to investigate the crystallographic relationship of the coating layer and the host material on the sides of the interface and their effect on the electrochemical performance.

Here, a thin LTO epitaxial coating layer is constructed on the surface of $LiMn_2O_4$ hollow microspheres (LMO) through a solvothermal assisted method. From high resolution transmission electron microscopy (HR-TEM) and high resolution high angle annular dark field scanning transmission electron microscopy (HAADF-STEM) images, it is first proved that the LTO coating layer is heteroepitaxial growth on LMO. In the epitaxial coating material (EC-LMO@LTO), each particle consists of a $LiMn_2O_4$ surrounded by a thin epitaxial LTO outer layer. For the LIB cathode, the cyclability, thermal and rate capability of EC-LMO@LTO are significantly improved not only at room temperature but also at elevated temperatures. The EC-LMO@LTO cathode achieves a capacity retention of 97.0% at 1 C (140 mA g^{-1}) after 100 charge/discharge cycles at room temperature. It delivers a discharge capacity of 110.4 mAh g^{-1} at a high current of 1680 mA g^{-1} (12 C), corresponding to a 313% improvement in reversible capacity compared with a bare LMO cathode under a severe test condition of 60 °C.

EXPERIMENTAL SECTION

Preparation of the Samples. First, $MnCO_3$ microspheres were obtained through the method reported before by our group.[35] The as-prepared $MnCO_3$ microspheres were decomposed at 400 °C for 5 h to obtain MnO_2 microspheres. Last, to obtain LMO, stoichiometric amounts of MnO_2 microspheres and $LiOH·H_2O$ were added to a certain amount of ethanol, forming a suspension. The mixture continued to stir until ethanol evaporated out at room temperature. Then, the mixture was calcined at 700 °C for 10 h in air.

Coating of TiO_2. 0.2 g of as-prepared LMO was dispersed into 15 mL of ethanol and then 0.02 g of $Ti(OC_4H_9)_4$ was added. The mixture was sealed in Teflon reactor and maintained at 150 °C for 5 h, obtaining a thin amorphous TiO_2 coating layer on the surface of LMO. The precursor was annealed at 700 °C for 2 h to obtain LMO@TiO_2 for comparison with EC-LMO@LTO.

Converting to EC-LMO@LTO. 0.2 g of the LMO with a thin amorphous TiO_2 coating layer was mixed with 0.002 g of $LiOH·H_2O$ in ethanol. The mixture continued to stir until the ethanol evaporated out at room temperature. Finally, the mixture was calcined at 700 °C for 2 h.

Characterization. The X-ray diffraction (XRD) patterns of the as-prepared samples were collected on a PANalytical X-pert diffractometer (PANalytical, The Netherlands) with Cu Kα radiation from 10 to 80°. Hitachi field-emission scanning electron microscopy (FE-SEM S-4800) was used to analyze the size and morphology of the samples. The elemental compositions were characterized using the energy dispersive spectroscopy (EDX) (Oxford INCA, Britain). The hollow microspheres and the coating layers were observed by transmission electron microscopy (HR-TEM and HAADF-STEM) (Tecnai G^2 F20). X-ray photoelectron spectroscopy (XPS) was conducted on a PHI Quanteral II (Japan) instrument and the energy scale was adjusted based on the graphite peak in the C 1s spectrum at 284.5 eV. The data were fitted using XPSPEAK41 program. The exact ratio of Li:Mn for LMO with amorphous titanium oxide coating layer after the solvothermal process was calculated using inductive coupled plasma atomic emission spectrometry (ICP-AES, ICAP-6300).

Electrochemical Tests. Electrochemical measurements were carried out using CR2025 coin cells. The electrodes were prepared by casting a slurry of 80 wt % the samples, 10 wt % carbon black and 10 wt % poly(vinylidene fluoride) (PVDF) binder in *N*-methyl-2-pyrrolidone (NMP) on aluminum foil. Then, the foil was dried in a vacuum at 120 °C for 12 h. The typical active material loading was approximately 2 mg cm^{-2} and the electrode thickness was measured to be 50 μm. The cells were assembled in an argon-filled glovebox (with O_2 < 1 ppm and H_2O < 1 ppm) using Li metal as the counter and reference electrodes. Celgard 2400 films were used as separators, and the electrolyte was a solution of 1 M $LiPF_6$ dissolved in ethyl carbonate/dimethylcarbonate/diethylcarbonate (EC/DMC/DEC) (1:1:1 v/v/v). The charge−discharge testing was performed galvanostatically between 3 and 4.5 V on a LAND CT-2001A cell test instrument at around 25 and 60 °C. The charge rates were equal to the discharge rates. The weights of the coating layer were also calculated within the active materials. When the charge/discharge rates were higher than 0.5 C, a constant voltage charge step was used for 30 min after the constant current charge step to reach the predetermined voltage. Cyclic voltammetry (CV) was conducted on IM6e electrochemical workstation in the potential range of 3−4.5 V (vs Li/Li^+) and at a scan rate of 0.1 mV s^{-1}. Electrochemical impedance spectroscopic (EIS) measurements were carried out using a two-electrode coin cells at room temperature with an IM6e electrochemical workstation over the frequency range between 100 kHz and 0.1 Hz and applying an AC signal of 5 mV.

The Li^+-ion diffusion coefficients calculated from EIS data according to the following equation[36]

$$D_{Li} = R^2T^2/2A^2F^4n^4C^2\sigma^2 \quad (1)$$

Where D_{Li} is the diffusion coefficient of Li^+ ions, R is the gas constant, T is the absolute temperature, A is the surface area of the positive electrode, F is the Faraday's constant, n is the number of transferred electron(s) per molecule during oxidization, C is the Li^+-ion concentration in cathode material and σ is the Warburg factor, which is obtained from the slope of Z' vs reciprocal square root of frequency in the low-frequency region ($\omega^{-1/2}$).

RESULTS AND DISCUSSION

In this paper, solvothermal processing is selected to construct the LTO epitaxial coating layer on the $LiMn_2O_4$ hollow spheres (LMO) surfaces. Scheme 1 illustrates the coating process and the evolution of the composite. First, LMO hollow microspheres were prepared using $MnCO_3$ as a self-template obtained through the method reported before by our group.[35] In this process, $MnCO_3$ microspheres are decomposed to highly porous MnO_2 at 400 °C due to the large weight lose and release of CO_2 during the heat treatment. After that, $LiOH·H_2O$ is introduced into the pores of MnO_2 driven by the capillary force during the impregnation of MnO_2 to $LiOH·H_2O$ solution. With calcination, LMO hollow spheres can be formed. This may result from the fusion of the pores in MnO_2 and an analogous to the Kirkendall effect, which refers to the formation of void due to unequal direction matter flows in a diffusion couple.[35,37] During lithiation, the fast outward diffusion of Mn atoms and the slow inward diffusion of O atoms form a hollow cavity in the LMO microspheres.[35,37] Then, a uniform amorphous titanium oxide coating layer was deposited on the surface of LMO by the reaction of $Ti(OC_4H_9)_4$ with the trace H_2O molecules in ethanol at 150 °C, which is confirmed by TEM. The exact ratio of Li:Mn measured by ICP-AES is 0.99:2.01 for LMO with amorphous titanium oxide coating layer. It can be illustrated that few of the Li ions dissolve in ethanol within the experimental error during the solvothermal process due to the short reaction time. Last, it could be converted into epitaxial LTO coating layer by reaction with LiOH under 700 °C. The formation of epitaxial LTO coating layer can be attributed to the low melting point of LiOH, leading to the easy diffusion of Li^+ ions to the amorphous titanium oxide layer during the calcination.[38] In addition, LMO with amorphous titanium oxide coating layer also calcined in air to obtained TiO_2-coated LMO ($LMO@TiO_2$) for comparison with EC-LMO@LTO to examine the effect of epitaxial coating layer on electrochemical performance.

The XRD patterns of the as-prepared samples are shown in Figure 1. All sharp reflections reveal the as-prepared materials

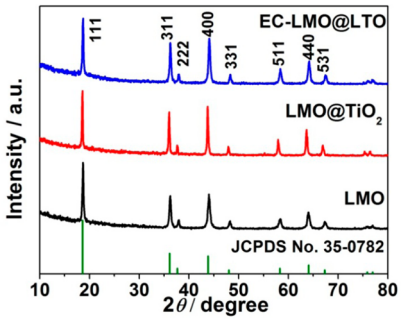

Figure 1. XRD patterns of LMO, $LMO@TiO_2$ and EC-LMO@LTO.

are well-crystallized. All the peaks can be assigned to the cubic spinel phase ($Fd\bar{3}m$), corresponding well to JCPDS data (35-0782). It should be noted that the XRD patterns of $LMO@TiO_2$ and EC-LMO@LTO are without any impurity phases, attributed to the low loading content of Ti-based compounds.[39] By increasing the TiO_2 content to 10 wt % for the $LMO@TiO_2$ sample, characteristic peaks for TiO_2 around 27.59, 41.43, 54.51 and 56.86° begin to appear (Supporting Information, Figure S1a). It may demonstrate that TiO_2 is deposited on the surface of LMO during the solvothermal and annealing process. When the large loading content of TiO_2 is converted to LTO by reaction with LiOH, the XRD pattern of 10 wt % coated LMO@LTO is the same as that of LMO. Meanwhile, the characteristic peaks of TiO_2 disappear (Supporting Information, Figure S1b), which illustrates that the TiO_2 on the surface of LMO is all converted to LTO. This is because LTO shares the same spinel structures with LMO having similar XRD peak sites, which can lead to the main diffraction peaks of LTO being superimposed by those of LMO.[40]

The morphologies and microstructures of LMO, $LMO@TiO_2$ and EC-LMO@LTO are shown in Figure 2. As it can be seen, LMO hollow microspheres are about 1 μm in size with a shell thickness of about 200 nm. It is clearly revealed that the shell is aggregated from approximately 100 nm primary nanoparticles. After solvothermal processing, a thin uniform coating of amorphous titanium oxide deposits on the surface of LMO, which could be observed by HR-TEM imaging (Supporting Information, Figure S2). The thickness of the coating layer is estimated to be about 5 nm. The size and hollow microspheres morphology of $LMO@TiO_2$ are all maintained through annealing. The unique difference is that the coating layer makes the surface of the microspheres smoother (Figure 2b,e). When the amorphous coating layer reacts with LiOH, the smooth surface of $LMO@TiO_2$ is changed to small nanoparticles, attributing to the different expansion of TiO_2 and LTO during annealing processing (Figure 2c,f).[41] In addition, the coating layers could not be easily identified because of the thinness of the shell. The coated samples were also confirmed by energy-dispersive X-ray (EDX) spectroscopy. The results of EDX show that Ti-based coating layer on the surface of LMO can be clearly observed, whereas the prepared LMO does not exhibit any titanium (Supporting Information, Figure S3). The element maps of EC-LMO@LTO from EDX spectroscopy are used to ascertain the distributions of titanium, manganese and oxygen (Supporting Information, Figure S4). Figure S4d (Supporting Information) shows that titanium is uniformly distributed on the surface of LMO.

Figure 3a shows a cross-section high-resolution transmission electron microscopy (HR-TEM) image of EC-LMO@LTO. As with epitaxial coating materials from the literature,[42] the interface between the coating layer and the host materials can be well-identified through the different contrast of LMO and LTO, which is distinguished by a white dashed line. The distinct contrast and lattice demonstrate the good epitaxial quality of LTO grown on LMO. The labeled *d*-spacing of 2.48 and 2.52 Å in the interior and the surface regions correspond to the lattice fringes of the (311) planes of LMO and LTO, respectively. Another lattice fringes marked by white arrows are assigned to the (400) planes of LMO (2.06 Å) and LTO (2.09 Å), respectively. Figure 3b shows the fast Fourier transform (FFT) pattern of the interface (Figure 3a), in which there are two close well-aligned sets of cubic spots assigned to LMO and LTO, respectively. The epitaxial relationships between the host materials (LMO) and the coating layer (LTO) determined from the HR-TEM and FFT images are $(311)_{LMO}//(311)_{LTO}$ and $(400)_{LMO}//(400)_{LTO}$. As shown in the HAADF-STEM image (Figure 3c), it can be easily distinguished the epitaxial coating layer and the host material through the distinct contrast.[21] To illustrate the variation of the composition more clearly, the results of corresponding EDX line scans at the interface are shown in Figure 3d. A small amount of Mn may diffuse to the LTO layer and a small amount Ti might diffuse to the LMO materials at the calcination temperature of 700 °C.

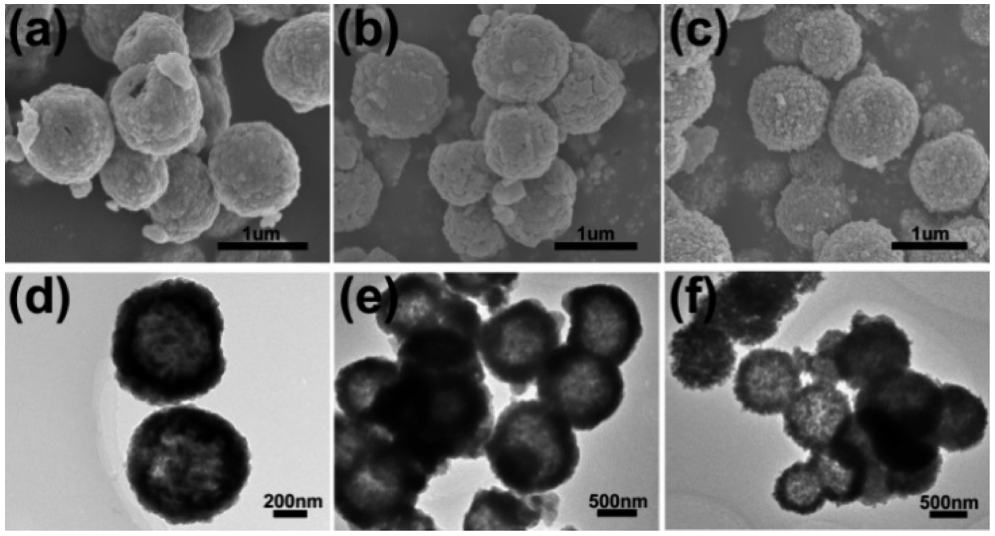

Figure 2. FE-SEM images of LMO (a), LMO@TiO_2 (b) and EC-LMO@LTO (c). TEM images of LMO (d), LMO@TiO_2 (e) and EC-LMO@LTO (f).

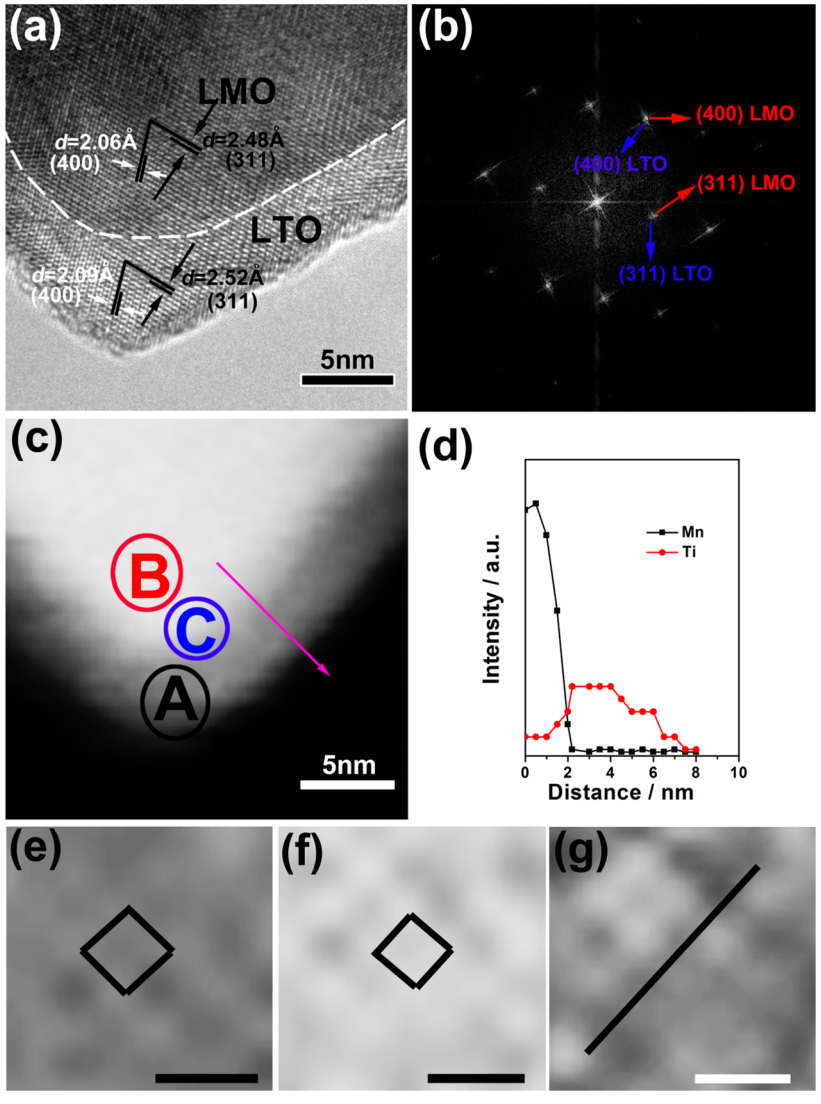

Figure 3. (a) HR-TEM image of EC-LMO@LTO, showing the interface of LMO and LTO. (b) Corresponding fast Fourier transform (FFT) pattern of panel a. (c) HAADF-STEM image of EC-LMO@LTO. (d) EDX line scan data collected at the interface through the arrow in panel c. (e–g) HAADF-STEM images with atomic resolution of the A (e), B (f) and C (g) regions in panel c, scale bar: 5 Å.

However, it can be clearly observed that the intensity of Mn element is dramatically declined nearly to zero and Ti is rapidly increased to the top value at the interface, which can illustrate that the LMO is mainly confined to the interior region, while LTO is only detected on the surface region. Combined with the results of HR-TEM and STEM, it can be determined that LTO is an epitaxial coating layer on LMO.

To clearly show the epitaxial coating layer, high-resolution STEM with an atomic scale at the interface for EC-LMO@LTO was measured. Figure 3e−g are the magnified STEM images with atomic scale corresponding to the A (the coating layer), B (the host material) and C (the interface) regions in Figure 3c, respectively. It can be clearly observed that the atoms are both arranged like a diamond shape in both A and B regions which is attributed to the same cubic spinel phase ($Fd\bar{3}m$) of the host material and the coating layer. The unique difference is the two different contrasts of the atoms in the two regions, which might be due to the different atomic number of Mn and Ti elements. The brighter ones can be assigned to Mn columns and the less bright ones are Ti columns. In addition, the two different contrasts also might be owing to the thickness effect. However, the sudden contrast changes in Figure 3g (the interface region) illustrate that the contrast difference can be due to not the thickness effect but the different atomic number Z of Mn and Ti elements. Furthermore, the atoms are connected directly without any defect showing the LTO epitaxial coating layer on the LMO host materials. The manganese atoms are arranged like a diamond shape with Mn columns showing two different contrasts (Figure 3f).[43,44] The Mn columns at the diamond vertices show a brighter contrast, which have an atomic density 2× that of the Mn columns with less bright contrast on the diamond edges along the $[04\text{-}4]_{cubic}$ direction. On the basis of the STEM analysis, the epitaxially coating layer LTO is constructed on the surface of the host material LMO with the same lattice orientation.

XPS was employed to characterize the surface element composition and oxidation state of LMO, LMO@TiO_2 and EC-LMO@LTO. Typical XPS survey scans are shown in Figure S5a (Supporting Information). In comparison with LMO, the XPS patterns of LMO@TiO_2 and EC-LMO@LTO show one more peaks at binding energies of 458 and 457.81 eV, both assigned to $2p_{3/2}$ of Ti^{4+} (Supporting Information, Figure S5b,c). Ti $2p_{3/2}$ in XPS spectrum of EC-LMO@LTO shifts to the lower binding energy compared to LMO@TiO_2, which is attributed to the influence of lithium ions.[39,40]

The electrochemical properties of LMO, LMO@TiO_2 and EC-LMO@LTO were initially investigated by cyclic voltammetry (CV). As shown in Figure S6 (Supporting Information), two pairs of typical redox peaks around 3.96/4.04 V and 4.10/4.17 V versus Li metal can be clearly observed for all the samples, suggesting that Li^+ ions are extracted from and inserted into the spinel phase in a two-step process. These are corresponding to a two-phase transition of $Li_{0.5}Mn_2O_4$/$LiMn_2O_4$ and λ-MnO_2/$Li_{0.5}Mn_2O_4$ versus Li/Li^+.[45] Compared to LMO and LMO@TiO_2, the CV curve of EC-LMO@LTO shows two anodic peaks at lower potentials and two cathodic peaks at higher potentials (Supporting Information, Table S1). It is demonstrated that LMO with surfaces modified by LTO can evidently diminish the polarization of LMO cathodes, which is helpful to improve the reversibility between charge and discharge processes. However, the peak currents for EC-LMO@LTO are less than those of LMO and LMO@TiO_2, which may be induced by low electronic conductivity of LTO film on the surface.[5] Additionally, the cyclic voltammetry of EC-LMO@LTO cathode from 1.0 to 2.0 V was also investigated (Supporting Information, Figure S7). There is an anodic peak at 1.66 V corresponding to the voltage platform of the charge process for spinel LTO,[46] which further certificates the coating layer is LTO.

LMO, LMO@TiO_2 and EC-LMO@LTO were used as the cathodes in half coin cells for the examination of the effects of epitaxial coating layer on the electrochemical performance of LMO. Cells were tested in the voltage range of 3−4.5 V and the charge rates were equal to the discharge rates. The weights of the coating layer were also calculated within the active materials. Figure 4a shows the first charge/discharge curves

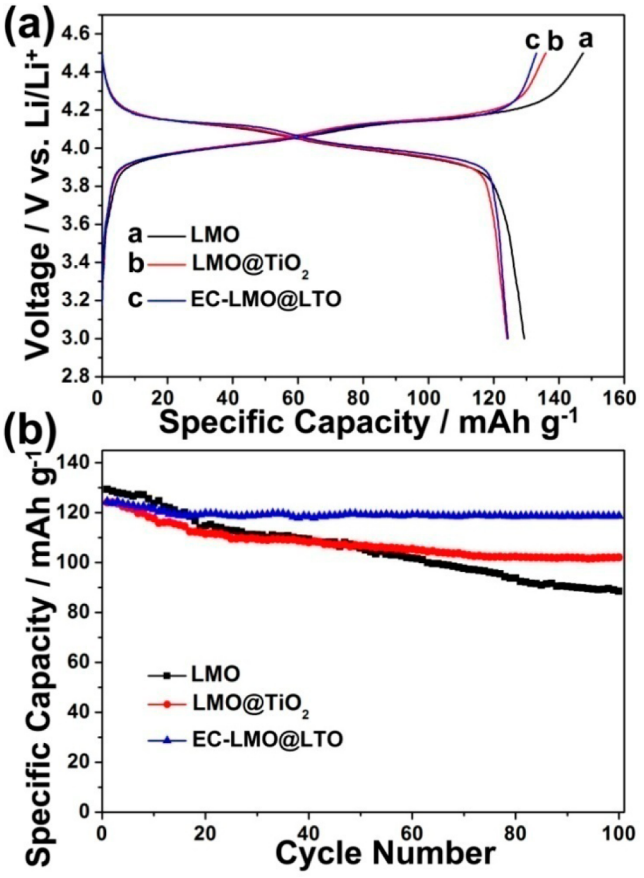

Figure 4. LMO, LMO@TiO_2 and EC-LMO@LTO cathodes cycled at 0.1 C (1 C = 140 mA g^{-1}) in the voltage window of 3−4.5 V at 25 °C. (a) Initial charge/discharge profiles. (b) Specific discharge capacity vs the cycle number.

of pristine LMO, LMO@TiO_2 and EC-LMO@LTO at 0.1 C (1 C = 140 mA g^{-1}) at 25 °C. As it can be seen, the first charge/discharge curves all present two characteristic voltage plateaus corresponding well to the redox peaks in the CV plots and in consistent with other reports.[6−20] The initial charge and discharge capacities of LMO cathode are 147.4 and 129.4 mAh g^{-1}, respectively. The initial irreversible capacity loss (ICL) is as high as 18 mAh g^{-1} and the Coulombic efficiency is only 87.8%. For LMO@TiO_2 and EC-LMO@LTO cathodes, the initial charge capacities are 136.0 and 133.1 mAh g^{-1}, respectively. The corresponding discharge capacities are 124.1 and 124.4 mAh g^{-1}, which are a little lower than uncoated LMO cathode observed in other coated cathodes.[17−19,29−34] However, the

dx.doi.org/10.1021/am504319y | ACS Appl. Mater. Interfaces 2014, 6, 18742−18750

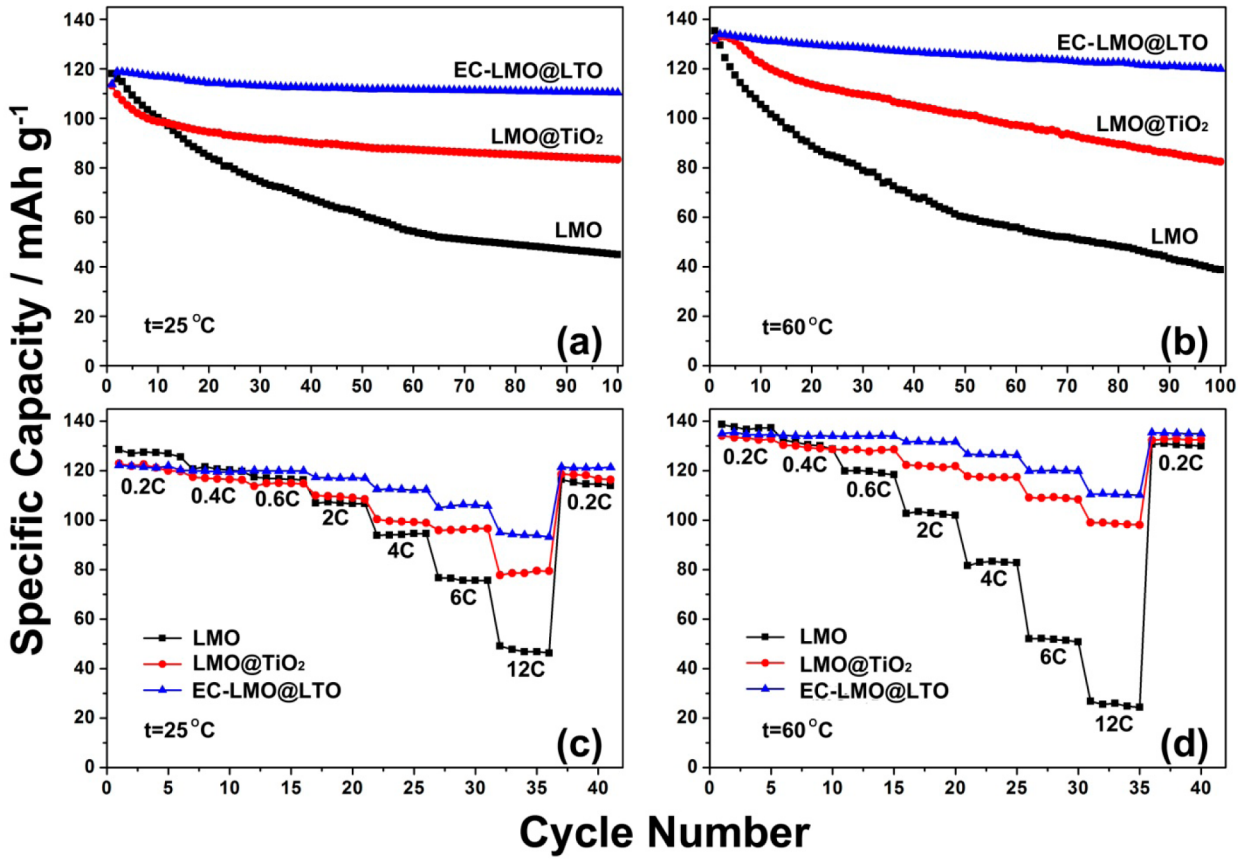

Figure 5. Cycling performances of as-prepared materials cycled at 1 C at 25 °C (a), 60 °C (b). Rate capabilities of LMO, LMO@TiO_2 and EC-LMO@LTO cathodes at 25 °C (c) and 60 °C (d).

Coulombic efficiencies rise to 91.3 and 93.5% and the ICL values drop to 11.9 and 8.7 mAh g^{-1} after surface modification by TiO_2 and LTO, respectively. The irreversible capacity at the initial cycle is owing to the formation of passivation on the surface of the LMO, the electrolyte decomposition and the Mn ions dissolution.[29−34] Comparing with the TiO_2 coating layer, LTO epitaxial coating layer is more beneficial to the reversible intercalation and deintercalation of Li^+ ions because it can more remarkably suppress these undesired reactions. Figure 4b shows comparative cycling stability of LMO, LMO@TiO_2 and EC-LMO@LTO cathodes at 0.1 C at 25 °C. After 100 charge/discharge cycles, the discharge capacity of EC-LMO@LTO cathode still maintains 118.7 mAh g^{-1}, which is larger than the 88.5 mAh g^{-1} of LMO and 102.1 mAh g^{-1} of LMO@TiO_2. The capacity retentions are 68.4, 82.3 and 95.4% for LMO, LMO@TiO_2 and EC-LMO@LTO cathodes, respectively, illustrating a more stable cycle life after epitaxial coating with LTO.

When the current density increases to 1 C (140 mA g^{-1}), the cycling performances of LMO, LMO@TiO_2 and EC-LMO@LTO cathodes were tested at room temperature (25 °C) and an elevated temperature (60 °C) (Figure 5a,b), respectively. The EC-LMO@LTO cathode delivers the best cyclability and the highest final capacity at either 25 or 60 °C. It is noteworthy that the discharge capacity gradually increases at the first five cycles and then decreases for the EC-LMO@LTO cathode, which can be recognized as the activation process for gradually opening the tunnel for the transportation of Li^+ ions.[30] The first discharge capacities of LMO, LMO@TiO_2 and EC-LMO@LTO cathodes are 118.1, 113.2 and 113.8 mAh g^{-1} at 25 °C. After 100 charge and discharge cycles, the discharge capacity for EC-LMO@LTO cathode is as high as 110.4 mAh g^{-1}, much more than the 44.9 mAh g^{-1} of uncoated LMO and 83.3 mAh g^{-1} of LMO@TiO_2. The corresponding capacity retentions are 38.0, 73.6 and 97.0% for LMO, LMO@TiO_2 and EC-LMO@LTO cathodes, respectively. When the temperature is set at 60 °C, the discharge capacities of the LMO, LMO@TiO_2 and EC-LMO@LTO cathodes increase to 135.3, 131.8 and 132.2 mAh g^{-1}. As shown in Figure 5b, the capacity of LMO cathode declines dramatically attributing to the dissolution of manganese ions rapidly and violent reaction between cathode and electrolyte at elevated temperature (60 °C). At the elevated temperature, LMO and LMO@TiO_2 show capacity retentions of 28.7 and 62.6% after 100 cycles, respectively. On the other hand, EC-LMO@LTO cathode exhibits 90.6% of capacity retention.

The rate capability can further highlight the advantage of the heteroepitaxial LTO coating. The comparative rate capabilities of LMO, LMO@TiO_2 and EC-LMO@LTO cathodes cycled from 0.2 to 12 C at 25 (Figure 5c) and 60 °C (Figure 5d). At all rates tested, except for 0.2 C, the EC-LMO@LTO cathode exhibited the highest capacities among the three cathodes at both temperatures. The surface modification cathode has a lower capacity than the uncoated cathode at low rates, in agreement with other coating samples.[10,18] Under room temperature (25 °C), the EC-LMO@LTO cathode delivers a discharge capacity of 122.2, 117.3, 112.5, 105 and 95 mAh g^{-1} at 0.2, 2, 4, 6 and 12 C, respectively. The capacity at 12 C for the EC-LMO@LTO cathode is corresponding to 77.7% of the capacity at 0.2 C, whereas the LMO and LMO@TiO_2 cathodes only retain 38.2 (49.1 mAh g^{-1}) and 63.3% (77.8 mAh g^{-1}),

respectively. Compared to the tests at room temperature, it is seen that LMO@TiO_2 and EC-LMO@LTO cathodes exhibit the increased discharge capacities at elevated temperature (60 °C). However, uncoated LMO cathode shows sharply capacity fading to 26.7 mAh g^{-1} at 12 C with capacity retention of 19.1% compared to 0.2 C. The discharge capacities for EC-LMO@LTO cathode at rates of 0.2, 2, 4, 6 and 12 C are 134.9, 131.7, 126.5, 120 and 110.4 mAh g^{-1}, respectively, which is higher than those of LMO@TiO_2 cathode. Compared to the rate capability at 25 °C, the EC-LMO@LTO cathode delivers not only improved rate capability but also increased initial discharge capacity at 60 °C. The increased discharge capacity can be attributed to the thermal effect at elevated temperature. It can generate volumetric expansion and improve conductivity of LTO coating layer, resulting in faster Li^+-ion diffusion and electron transition at high kinetics.[10] When the current density is decreased from 12 to 0.2 C, the capacity recoveries for the EC-LMO@LTO cathode at both temperatures are 100%, indicating that the epitaxial LTO coating layer can effectively minimize structural distortion at the surface of the particle. Capacity recoveries of LMO and LMO@TiO_2 cathodes are 91.0 and 96.0%, respectively, showing possible structural degradation during high rate cycling.[6]

Compared to other coating $LiMn_2O_4$ cathodes,[6−20] the EC-LMO@LTO cathode demonstrates better stable cycling life, thermal performance and rate capability under a high cutoff voltage, which can be attributed to the heteroepitaxial LTO coating layer on the surface of LMO. First, the LTO coating layer can prevent direct contact between LMO and organic electrolyte, which can effectively reduce the side reactions (the decomposition of the electrolyte and the scavenging of HF from the electrolyte), suppress the tendency for Mn dissolution and eliminate the structural distortion at the surface, especially at elevated temperatures. Because the side reactions and the Mn dissolution during cycling can result in deposition of resistive components (such as LiF) on the electrode surface suppressing the migration of Li^+ ions and electron and the loss of active materials, which may cause capacity fading. Second, the strong adhesion to the host material of the epitaxial LTO coating layer grown on LMO enables the structure more stable when cycling. Conversely, the coating layer with weak bonding maybe easily loosen up or peel off from the active material causing the loss of pathway for Li^+ ions and electron transfer. Third, the same spinel structure and small lattice mismatch of LTO and LMO can eliminate the phase interface and stacking faults leading to an efficient channel for Li^+-ion diffusion comparing with usual TiO_2-coated cathode as a reference. In addition, much higher Li^+-ion mobility in LTO makes the transportation of Li^+ ions to the internal active material easier.

Electrochemical impedance spectroscopy (EIS) of LMO, LMO@TiO_2 and EC-LMO@LTO was conducted to further investigate the effect on electrochemical performances of the epitaxial coating layer. The Nyquist plots of all samples obtained before and after 100 charge/discharge cycles at 1 C are displayed in Figure S8 (Supporting Information), which are fitted by the same equivalent circuit (inset of Figure S8a, Supporting Information) and the fitted results are listed in Table S2 (Supporting Information). Before cycling, the EC-LMO@LTO cathode displays the largest Re (combined impedance of the electrolyte and cell components), which may result from the low electronic conductivity of LTO coating on LMO.[5,17] The increase of Re values with cycling is due to the precipitation of resistive components (such as LiF) on the electrode surface.[19] The smallest Re value after 100 cycles for EC-LMO@LTO illustrates that the deposition of resistive components can be largely prohibited by LTO layer. The charge transfer resistances (Rct) for EC-LMO@LTO are much smaller than those for the uncoated and TiO_2 coated LMO, which indicates that epitaxial coating layer can more effectively reduce the barrier for Li^+-ion transfer at the electrode−electrolyte interface than the simple physical TiO_2 coating layer. After 100 cycles at 1 C, the values of Rct increase to 500.4, 275.5 and 178.1 Ω with the increments of 239.5, 106.8 and 55.7 Ω for uncoated LMO, LMO@TiO_2 and EC-LMO@LTO, respectively. Compared with uncoated LMO and LMO@TiO_2, the smallest Rct value and increment during insertion and extraction of Li^+ ions can be attributed to dramatically suppressing the dissolution of manganese, protecting the active material from reacting with electrolyte and restricting the thickening of SEI film during the charge−discharge process by the LTO coating layer.[19] Besides, the Li^+-ion diffusion coefficients (Supporting Information, Table S3) of all three samples calculated from EIS data according to eq 1. Among them, the Li^+-ion diffusion coefficient of EC-LMO@LTO is about 3 times larger than that of the TiO_2-coated cathode, which further proves that epitaxial LTO coating layer can form more efficient paths for Li^+-ion diffusion. The superior rate performance and the obviously reduced charge transfer resistance of EC-LMO@LTO are owing to the thin unique epitaxial coating layer on the surface, strong adhesion to host material with the same lattice orientation and favorable tunnel for Li^+-ion diffusion.

To further confirm the good cycling stability of EC-LMO@LTO, we opened the cycled cells and did SEM observations for LMO, LMO@TiO_2 and EC-LMO@LTO cathodes. Figure S9 (Supporting Information) shows the morphology of these samples after 100 charge and discharge cycles at 1 C. It can be seen that the hollow spheres of uncoated LMO split (marked by arrows in Figure S9a, Supporting Information). The pulverization may be attributed to the side reactions with the cycle increasing leading to the obvious capacity decay for uncoated LMO cathode.[20] The LMO coated by TiO_2 and LTO can retain their initial hollow spherical morphology with no evident change, supporting the better cycle performance of LMO@TiO_2 and EC-LMO@LTO than uncoated LMO.

CONCLUSION

In conclusion, LTO is first used as an epitaxial coating layer on the $LiMn_2O_4$ hollow sphereical surface through a solvothermal assisted processing. The good heteroepitaxial relationship is confirmed by HR-TEM and STEM. The EC-LMO@LTO cathode exhibits an impressive rate capability as well as cycling stability, especially at elevated temperatures, benefiting from the epitaxial coating layer. In the epitaxial coating material, each particle consists of a $LiMn_2O_4$ surrounded by an epitaxial LTO outer layer that leads to strong bonding with the host material. It can effectively suppress the electrochemical side reactions on the active materials surface. The small lattice mismatch and high Li^+-ion mobility can guarantee a favorable and fast pathway for Li^+-ion transfer. All of these results indicate that the cathode with an epitaxial coating layer can greatly optimize the performance to satisfy the requirements for HEVs and other power tools. Furthermore, it is postulated that the novel epitaxial coating strategy can be applied to design and development of a wide range of other high performance electrode materials.

■ ASSOCIATED CONTENT

Supporting Information

XRD curves of 10 wt % TiO_2 and LTO coating samples; HR-TEM of precursor before annealing; EDX, SEM and mapping, and XPS results of EC-LMO@LTO; CV curves at 3−4.5 V; EIS before and after 100 cycles; CV curve of EC-LMO@LTO at 1−2 V; SEM after 100 cycles. This material is available free of charge via the Internet at http://pubs.acs.org.

■ AUTHOR INFORMATION

Corresponding Author

*C. Cao. E-mail: cbcao@bit.edu.cn.

Notes

The authors declare no competing financial interest.

■ ACKNOWLEDGMENTS

This work was supported financially by the grant from the National Natural Science Foundation (NNSF) of China (No. 21371023).

■ REFERENCES

(1) Lee, S.; Cho, Y.; Song, H.-K.; Lee, K. T.; Cho, J. Carbon-Coated Single-Crystal $LiMn_2O_4$ Nanoparticle Clusters as Cathode Material for High-Energy and High-Power Lithium-Ion Batteries. *Angew. Chem., Int. Ed.* **2012**, *51*, 8748−8752.

(2) Kim, J.-S.; Kim, K. S.; Cho, W.; Shin, W. H.; Kanno, R.; Choi, J. W. A Truncated Manganese Spinel Cathode for Excellent Power and Lifetime in Lithium-Ion Batteries. *Nano Lett.* **2012**, *12*, 6358−6365.

(3) Okubo, M.; Mizuno, Y.; Yamada, H.; Kim, J.; Hosono, E.; Zhou, H. S.; Kudo, T.; Honma, I. Fast Li-Ion Insertion into Nanosized $LiMn_2O_4$ without Domain Boundaries. *ACS Nano* **2010**, *4*, 741−752.

(4) Lee, K. T.; Jeong, S.; Cho, J. Roles of Surface Chemistry on Safety and Electrochemistry in Lithium Ion Batteries. *Acc. Chem. Res.* **2013**, *46*, 1161−1170.

(5) Su, L. W.; Jing, Y.; Zhou, Z. Li Ion Battery Materials with Core−Shell Nanostructures. *Nanoscale* **2011**, *3*, 3967−3983.

(6) Cho, J. VO_x-Coated $LiMn_2O_4$ Nanorod Clusters for Lithium Battery Cathode Materials. *J. Mater. Chem.* **2008**, *18*, 2257−2261.

(7) Zhao, J. Q.; Wang, Y. Surface Modifications of Li-Ion Battery Electrodes with Various Ultrathin Amphoteric Oxide Coatings for Enhanced Cycleability. *J. Solid State Electrochem.* **2013**, *17*, 1049−1058.

(8) Lim, S.; Cho, J. PVP-Functionalized Nanometre Scale Metal Oxide Coatings for Cathode Materials: Successful Application to $LiMn_2O_4$ Spinel Nanoparticles. *Chem. Commun.* **2008**, 4472−4474.

(9) Guan, D. S.; Jeevarajan, J. A.; Wang, Y. Enhanced Cycleability of $LiMn_2O_4$ Cathodes by Atomic Layer Deposition of Nanosized-Thin Al_2O_3 Coatings. *Nanoscale* **2011**, *3*, 1465−1469.

(10) Zhao, J. Q.; Qu, G. Y.; Flake, J. C.; Wang, Y. Low Temperature Preparation of Crystalline ZrO_2 Coatings for Improved Elevated-Temperature Performances of Li-Ion Battery Cathodes. *Chem. Commun.* **2012**, *48*, 8108−8110.

(11) Walz, K. A.; Johnson, C. S.; Genthe, J.; Stoiber, L. C.; Zeltner, W. A.; Anderson, M. A.; Thackeray, M. M. Elevated Temperature Cycling Stability and Electrochemical Impedance of $LiMn_2O_4$ Cathodes with Nanoporous ZrO_2 and TiO_2 Coatings. *J. Power Sources* **2010**, *195*, 4943−4951.

(12) Yu, L. H.; Qiu, X. P.; Xi, J. Y.; Zhu, W. T.; Chen, L. Q. Enhanced High-Potential and Elevated-Temperature Cycling Stability of $LiMn_2O_4$ Cathode by TiO_2 Modification for Li-Ion Battery. *Electrochim. Acta* **2006**, *51*, 6406−6411.

(13) Zhang, Z. R.; Gong, Z. L.; Yang, Y. Electrochemical Performance and Surface Properties of Bare and TiO_2-Coated Cathode Materials in Lithium-Ion Batteries. *J. Phys. Chem. B* **2004**, *108*, 17546−17552.

(14) Tu, J.; Zhao, X. B.; Xie, J.; Cao, G. S.; Zhuang, D. G.; Zhu, T. J.; Tu, J. P. Enhanced Low Voltage Cycling Stability of $LiMn_2O_4$ Cathode by ZnO Coating for Lithium Ion Batteries. *J. Alloys Compd.* **2007**, *432*, 313−317.

(15) Liu, H. W.; Cheng, C. X.; Hu, Z. Q.; Zhang, K. L. The Effect of ZnO Coating on $LiMn_2O_4$ Cycle Life in High Temperature for Lithium Secondary Batteries. *Mater. Chem. Phys.* **2007**, *101*, 276−279.

(16) Qing, C. B.; Bai, Y.; Yang, J. M.; Zhang, W. F. Enhanced Cycling Stability of $LiMn_2O_4$ Cathode by Amorphous $FePO_4$ Coating. *Electrochim. Acta* **2011**, *56*, 6612−6618.

(17) Wang, Y. P.; Wang, X. Y.; Yang, S. Y.; Shu, H. B.; Wei, Q. L.; Wu, Q.; Bai, Y. S.; Hu, B. Effect of MgF_2 Coating on the Electrochemical Performance of $LiMn_2O_4$ Cathode Materials. *J. Solid State Electrochem.* **2012**, *16*, 2913−2920.

(18) Zhao, S.; Bai, Y.; Chang, Q. J.; Yang, Y. Q.; Zhang, W. F. Surface Modification of Spinel $LiMn_2O_4$ with FeF_3 for Lithium Ion Batteries. *Electrochim. Acta* **2013**, *108*, 727−735.

(19) Chen, Q. Q.; Wang, Y. B.; Zhang, T. T.; Yin, W. M.; Yang, J. W.; Wang, X. Y. Electrochemical Performance of LaF_3-Coated $LiMn_2O_4$ Cathode Materials for Lithium Ion Batteries. *Electrochim. Acta* **2012**, *83*, 65−72.

(20) Lee, S.; Jeong, M.; Cho, J. Optimized 4-V Spinel Cathode Material with High Energy Density for Li-Ion Cells Operating at 60 °C. *Adv. Energy Mater.* **2013**, *3*, 1623−1629.

(21) Sun, Y.-K.; Lee, M.-J.; Yoon, C. S.; Hassoun, J.; Amine, K.; Scrosati, B. The Role of AlF_3 Coatings in Improving Electrochemical Cycling of Li-Enriched Nickel-Manganese Oxide Electrodes for Li-Ion Batteries. *Adv. Mater.* **2012**, *24*, 1192−1196.

(22) Sun, Y.-K.; Myung, S.-T.; Park, B.-C.; Prakash, J.; Belharouak, I.; Amine, K. High-Energy Cathode Material for Long-Life and Safe Lithium Batteries. *Nat. Mater.* **2009**, *8*, 320−324.

(23) Huang, X.; Wang, M.; Willinger, M.-G.; Shao, L. D.; Su, D. S.; Meng, X.-M. Assembly of Three-Dimensional Hetero-Epitaxial ZnO/ZnS Core/Shell Nanorod and Single Crystalline Hollow ZnS Nanotube Arrays. *ACS Nano* **2012**, *6*, 7333−7339.

(24) Zhang, Y. Y.; Haberkorn, N.; Ronning, F.; Wang, H. Y.; Mara, N. A.; Zhuo, M. J.; Chen, L.; Lee, J. H.; Blackmore, K. J.; Bauer, E.; Burrell, A. K.; McCleskey, T. M.; Hawley, M. E.; Schulze, R. K.; Civale, L.; Tajima, T.; Jia, Q. X. Epitaxial Superconducting δ-MoN Films Grown by a Chemical Solution Method. *J. Am. Chem. Soc.* **2011**, *133*, 20735−20737.

(25) Yu, L.; Wu, H. B.; Lou, X. W. Mesoporous $Li_4Ti_5O_{12}$ Hollow Spheres with Enhanced Lithium Storage Capability. *Adv. Mater.* **2013**, *25*, 2296−2300.

(26) Li, N.; Zhou, G. M.; Li, F.; Wen, L.; Cheng, H.-M. A Self-Standing and Flexible Electrode of $Li_4Ti_5O_{12}$ Nanosheets with a N-Doped Carbon Coating for High Rate Lithium Ion Batteries. *Adv. Funct. Mater.* **2013**, *23*, 5429−5435.

(27) Feckl, J. M.; Fominykh, K.; Dcblinger, M.; Fattakhova-Rohlfing, D.; Bein, T. Nanoscale Porous Framework of Lithium Titanate for Ultrafast Lithium Insertion. *Angew. Chem.* **2012**, *124*, 7577−7581; *Angew. Chem., Int. Ed.* **2012**, *51*, 7459−7463.

(28) Shen, L.; Zhang, X.; Uchaker, E.; Yuan, C.; Cao, G. $Li_4Ti_5O_{12}$ Nanoparticles Embedded in a Mesoporous Carbon Matrix as a Superior Anode Material for High Rate Lithium Ion Batteries. *Adv. Energy Mater.* **2012**, *2*, 691−698.

(29) Yi, T.-F.; Shu, J.; Zhu, Y.-R.; Zhou, A.-N.; Zhu, R.-S. Structure and Electrochemical Performance of $Li_4Ti_5O_{12}$-Coated $LiMn_{1.4}Ni_{0.4}Cr_{0.2}O_4$ Spinel as 5 V Materials. *Electrochem. Commun.* **2009**, *11*, 91−94.

(30) Yi, T.-F.; Shu, J.; Yue, C.-B.; Zhu, X.-D.; Zhou, A.-N.; Zhu, Y.-R.; Zhu, R.-S. Enhanced Cycling Stability of Microsized $LiCoO_2$ Cathode by $Li_4Ti_5O_{12}$ Coating for Lithium Ion Battery. *Mater. Res. Bull.* **2010**, *45*, 456−459.

(31) Zhu, Y.-R.; Yi, T.-F.; Zhu, R.-S.; Zhou, A.-N. Increased Cycling Stability of $Li_4Ti_5O_{12}$-Coated $LiMn_{1.5}Ni_{0.5}O_4$ as Cathode Material for Lithium-Ion Batteries. *Ceram. Int.* **2013**, *39*, 3087−3094.

(32) Yao, J.; Shen, C.; Zhang, P.; Ma, C. A.; Gregory, D. H.; Wang, L. Spinel-$Li_{3.5+x}Ti_5O_{12}$ Coated $LiMn_2O_4$ with High Surface Mn Valence

for an Enhanced Cycling Performance at High Temperature. *Electrochem. Commun.* **2013**, *31*, 92−95.
(33) Liu, D.-Q.; Liu, X.-Q.; He, Z.-Z. The Elevated Temperature Performance of $LiMn_2O_4$ Coated with $Li_4Ti_5O_{12}$ for Lithium Ion Battery. *Mater. Chem. Phys.* **2007**, *105*, 362−366.
(34) He, Z.-Q.; Xiong, L.-Z.; Wu, X.-M.; Chen, S.; Huang, K.-L. Synthesis and Electrochemical Properties of $LiMn_2O_4/Li_4Ti_5O_{12}$ Composite. *Trans. Nonferrous Met. Soc. China* **2010**, *20*, s257−s261.
(35) Li, J. L.; Cao, C. B.; Xu, X. Y.; Zhu, Y. Q.; Yao, R. M. $LiNi_{1/3}Co_{1/3}Mn_{1/3}O_2$ Hollow Nano-Micro Hierarchical Microspheres with Enhanced Performances as Cathodes for Lithium-Ion Batteries. *J. Mater. Chem. A* **2013**, *1*, 11848−11852.
(36) Gao, P.; Li, Y. H.; Liu, H. D.; Pinto, J.; Jiang, X. F.; Yanga, G. Improved High Rate Capacity and Lithium Diffusion Ability of $LiNi_{1/3}Co_{1/3}Mn_{1/3}O_2$ with Ordered Crystal Structure. *J. Electrochem. Soc.* **2012**, *159*, A506−A513.
(37) Zhou, L.; Zhou, X. F.; Huang, X. D.; Liu, Z. P.; Zhao, D. Y.; Yao, X. D.; Yu, C. Z. Designed Synthesis of $LiMn_2O_4$ Microspheres with Adjustable Hollow Structures for Lithium-Ion Battery Applications. *J. Mater. Chem. A* **2013**, *1*, 837−842.
(38) Cho, Y.; Lee, S.; Lee, Y.; Hong, T.; Cho, J. Spinel-Layered Core-Shell Cathode Materials for Li-Ion Batteries. *Adv. Energy Mater.* **2011**, *1*, 821−828.
(39) Lu, J.; Peng, Q.; Wang, W. Y.; Nan, C. Y.; Li, L. H.; Li, Y. D. Nanoscale Coating of $LiMO_2$ (M = Ni, Co, Mn) Nanobelts with Li^+-Conductive Li_2TiO_3: Toward Better Rate Capabilities for Li-Ion Batteries. *J. Am. Chem. Soc.* **2013**, *135*, 1649−1652.
(40) Haetge, J.; Hartmann, P.; Brezesinski, K.; Janek, J.; Brezesinski, T. Ordered Large-Pore Mesoporous $Li_4Ti_5O_{12}$ Spinel Thin Film Electrodes with Nanocrystalline Framework for High Rate Rechargeable Lithium Batteries: Relationships among Charge Storage, Electrical Conductivity, and Nanoscale Structure. *Chem. Mater.* **2011**, *23*, 4384−4393.
(41) Ji, G.; Ma, Y.; Ding, B.; Lee, J. Y. Improving the Performance of High Capacity Li-Ion Anode Materials by Lithium Titanate Surface Coating. *Chem. Mater.* **2012**, *24*, 3329−3334.
(42) Tsuji, M.; Miyamae, N.; Lim, S.; Kimura, K.; Zhang, X.; Hikino, S.; Nishio, M. Crystal Structures and Growth Mechanisms of Au@Ag Core-Shell Nanoparticles Prepared by the Microwave-Polyol Method. *Cryst. Growth Des.* **2006**, *6*, 1801−1807.
(43) Huang, R.; Ikuhara, Y. H.; Mizoguchi, T.; Findlay, S. D.; Kuwabara, A.; Fisher, C. A. J.; Moriwake, H.; Oki, H.; Hirayama, T.; Ikuhara, Y. Oxygen-Vacancy Ordering at Surfaces of Lithium Manganses (III, IV) Oxide Spinel Nanoparticles. *Angew. Chem., Int. Ed.* **2011**, *50*, 3053−3057.
(44) Lee, M.-J.; Lee, S.; Oh, P.; Kim, Y.; Cho, J. High Performance $LiMn_2O_4$ Cathode Materials Grown with Epitaxial Layered Nanostructure for Li-Ion Batteries. *Nano Lett.* **2014**, *14*, 993−999.
(45) Deng, Y. F.; Zhou, Y. B.; Shi, Z. C.; Zhou, X.; Quan, X.; Chen, G. H. Porous $LiMn_2O_4$ Microspheres Exhibit High Rate Capability and Long-Term Cyclability as Cathode Materials for LIBs. *J. Mater. Chem. A* **2013**, *1*, 8170−8177.
(46) Rahman, Md. M.; Wang, J.-Z.; Hassan, M. F.; Wexler, D.; Liu, H. K. Amorphous Carbon Coated High Grain Boundary Density Dual Phase $Li_4Ti_5O_{12}$-TiO_2: A Nanocomposite Anode Material for Li-Ion Batteries. *Adv. Energy Mater.* **2011**, *1*, 212−220.